www.lajss.org
Latin American Journal of Solids and Structures 3 (2006) 59–73

Behaviour of an automotive bumper beam-longitudinal system at 40% offset impact: an experimental and numerical study

Satyanarayana Kokkula[a,*], Magnus Langseth[a],
Odd Sture Hopperstad[a] & Odd Geir Lademo[a,b]

[a]Structural Impact Laboratory (SIMLab), Department of Structural Engineering, Norwegian University of Science and Technology, NO-7491 Trondheim, Norway
[b]SINTEF Materials and Chemistry, Applied Mechanics and Corrosion, NO-7465 Trondheim, Norway

Abstract

Assessing the impact performance of bumper beam systems through a full-scale crash test of a car is not easy. Therefore, in the present study a bumper beam connected to two longitudinals was tested at 40% offset impact. Longitudinals of two different alloys (AA7003 and AA6060) and two tempers (T79 and T1) were tested, while using a single alloy (AA7108 – T6) for the bumper beam. The bumper beam is a box-like structure produced from an aluminium extrusion that is plastically formed to the required curvature by stretch-bending in a soft condition, which is obtained by soft solid-solution heat treatment. Subsequently, the bumpers are artificially age-hardened to T6 peak hardness condition. With an objective to develop modelling tools for an automotive bumper system subjected to impact loading conditions this paper presents both the experimental and numerical results. Experiments were performed using SIMLab's kicking machine to provide high-precision data for validation of numerical computations. The numerical study was carried out with the non-linear finite element code LS-DYNA, searching for an efficient, numerically robust and accurate representation of the observed system behaviour. For this purpose a user-defined elasto-viscoplastic material model was adopted, which incorporates state-of-the-art anisotropic plasticity, an isotropic strain and strain-rate hardening rule as well as some ductile failure criteria. The obtained differences in energy absorption and failure modes caused by varying the alloy and temper of the longitudinals are discussed in some detail.

1 Introduction

In modern cars, aluminium alloys are employed in the front and rear bumper beams, crashboxes, longitudinals and other safety components such as side-door impact beams, frames, engine cradles, chassis and suspension components. When using aluminium in the body structure of a vehicle, significant weight savings may be possible compared with the conventional steel structures, which will reduce fuel consumption and consequently lower carbon dioxide emissions. The

*Corresp. author Email: satyanarayana.kokkula@gmail.com Received 8 Aug. 2005; Revised: 13 Dec. 2005

Notation

f	Yield function
$\bar{f}$	Convex function
σ_0	Reference yield stress
$R(\bar{\varepsilon})$	Strain-hardening variable
$\bar{\varepsilon}$	Accumulated plastic strain
Q_{Ri}, C_{Ri}	Strain hardening constants in Voce rule
CTS	Critical thickness strain
α	Direction
$a_1, a_2, ..., a_8$	Dimensionless anisotropy parameters in *Yld2003*
$\boldsymbol{\sigma}$	Stress tensor

crash situations with which the automotive industry deals are of large variety; of these frontal offset impacts are the most commonly seen accidental situations on roads [5]. Bumper beam systems are one of the main structures for absorbing the collision energy in the event of an automobile crash. In a frontal or rear crash, the bumper beam is the primary component which undergoes damage and transfers the forces to the rest of the structure. Thus, the bumper beam systems play a prominent role in the passive safety of an automobile. Furthermore, the automotive producers are demanding for robust bumper beam systems showing good and reproducible impact behaviour.

Aluminium extrusions make it possible to design the regions at the front and rear end of the car to crush in a controlled fashion. The philosophy behind the crash management calls for the bumper beam system to take on as much of the energy from the impact as possible, and transferring as little deformation as possible further into the vehicle. Studying the impact behaviour of the bumper beam system is not trivial in the event of a full-scale crash test of a car. It is worth to note, however, conducting a full-scale crash test of a car is always time consuming and expensive. The paper summarizes the experimental and numerical results on the bumper beam-longitudinal systems subjected to 40% offset impact, that are presented in [3], [12] and [13]. The bumper beam system in this study consists of a bumper beam directly connected to a longitudinal at both ends, here after called a bumper beam-longitudinal system. That is, the system does not include any crashboxes.

2 Experimental programme

The configuration of the bumper beam-longitudinal system that was tested is shown in Figure 1(a). In this figure the cross-sectional dimensions of the longitudinal are also given. The cross-section details of the bumper beam and interface plate are given in Figure 1(b) and (c), respectively. The bumper beam was connected to the longitudinals by using M12 bolts via an interface plate, while the interface plates were MIG welded to the longitudinals. During testing

the impact velocity and the free length of the longitudinals were kept constant at 10 m/s (36 km/h) and 650 mm respectively. The trolley had a mass of 794 kg and thus the input kinetic energy was also kept constant at 39.7 kJ. Table 1 shows a summary of the tests carried out. As seen in Table 1 the main variable during testing was the strength of the longitudinals which was related to the observed difference in the stress-strain curves, Figure 9(a). The AA7003-T1 alloy (medium strength longitudinal) has a lower yield stress than the AA7003-T79 alloy (high strength longitudinal) but a considerable higher ultimate load carrying capability, as shown in Figure 9(a). It should be noted that the difference between high, medium and low strength longitudinals, in the present context, is related to the magnitude of the yield stress.

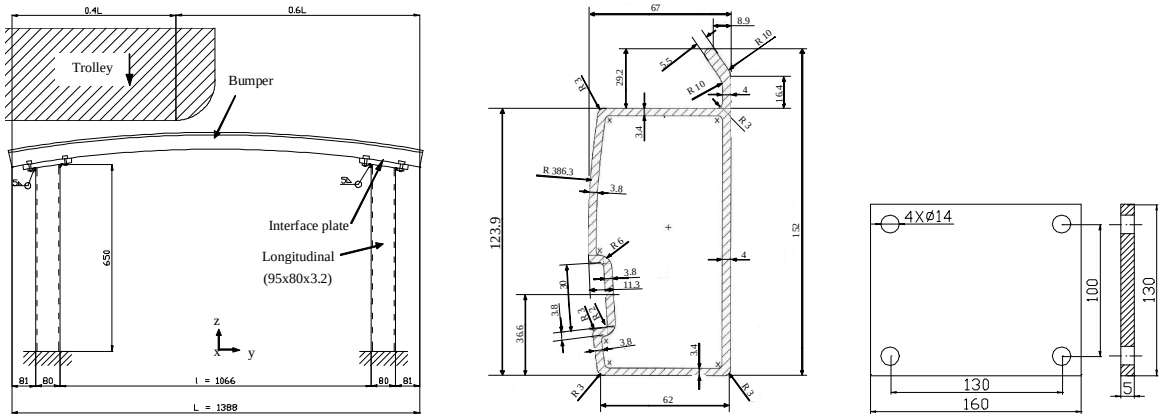

(a) (b) (c)

Figure 1: Bumper beam-longitudinal system at 40% offset impact, (a) schematic representation of the experimental test set-up, (b) cross-section details of bumper beam and (c) details of interface plate.

3 Experimental set-up

Experiments were performed using SIMLab's kicking machine [6] and is illustrated in Figure 2. An arm accelerates the trolley up to the desired impact velocity, after which the trolley traverses the length of the rails and hits the test specimen located at the far end. The impact velocity of the trolley is measured by means of a photocell system located directly in front of the test specimen. A high-speed video camera records the event at approximately 1100 frames per second. In case the test specimen does not have enough capacity to absorb all the kinetic energy of the trolley by itself, a secondary energy absorbing system is required. For this reason the trolley has rigid buffer plates on both sides of the loadcell. These buffer plates hit crash boxes fixed to the reaction wall, which ensure the integrity of the loadcells.

In the present study two loadcells were employed on the trolley and one loadcell at each

end of the longitudinals. The loadcells have strain gauges applied for the measurement of the impacting force as a function of time. The loadcells measure the axial force as well as two orthogonal bending moments. The acceleration, velocity and displacement histories of the trolley are obtained from the total force signal of the loadcells on the trolley; all the necessary calculations are presented in [6]. A sampling frequency of 500 kHz was used for the force signal in all the tests. The force signal has been filtered by a moving-point average algorithm, roughly corresponding to a low-pass filter with a cut-off frequency of 400 Hz. The moving-point average algorithm will reduce the oscillations in force level, but the absorbed energy will be correctly estimated.

Table 1: Test matrix for testing bumper beam-longitudinal system at 40% offset impact.

Test Series	Longitudinals	Impact velocity (m/s)
A1 **A2** **A3** **A4** **A5**	AA7003–T79 (High Strength)	10
B1 **B2** **B3**	AA7003–T1 (Medium Strength)	10
C1 **C2** **C3**	AA6060–T1 (Low Strength)	10
Bumper beam in alloy AA7108–T6		

4 Test results

In 40% offset impacts the bumper beam undergoes considerable bending due to the direct impact of the trolley. Furthermore, the energy absorption is mainly concentrated to the impacted end i.e. the left longitudinal, Figure 1(a). In the right longitudinal only minor deformations are observed. Test results of bumper beam-longitudinal systems at 40% offset impact when using high, medium and low strength longitudinals are discussed by the authors in [7–9] and are summarized in the following.

4.1 High strength longitudinals

According to Table 1, five repetitive tests were carried out using high strength longitudinals. The deformed configuration of the bumper beam-longitudinal system for test specimen **A1** along with the non-filtered and filtered force-deformation plots are shown in Figure 3. All the

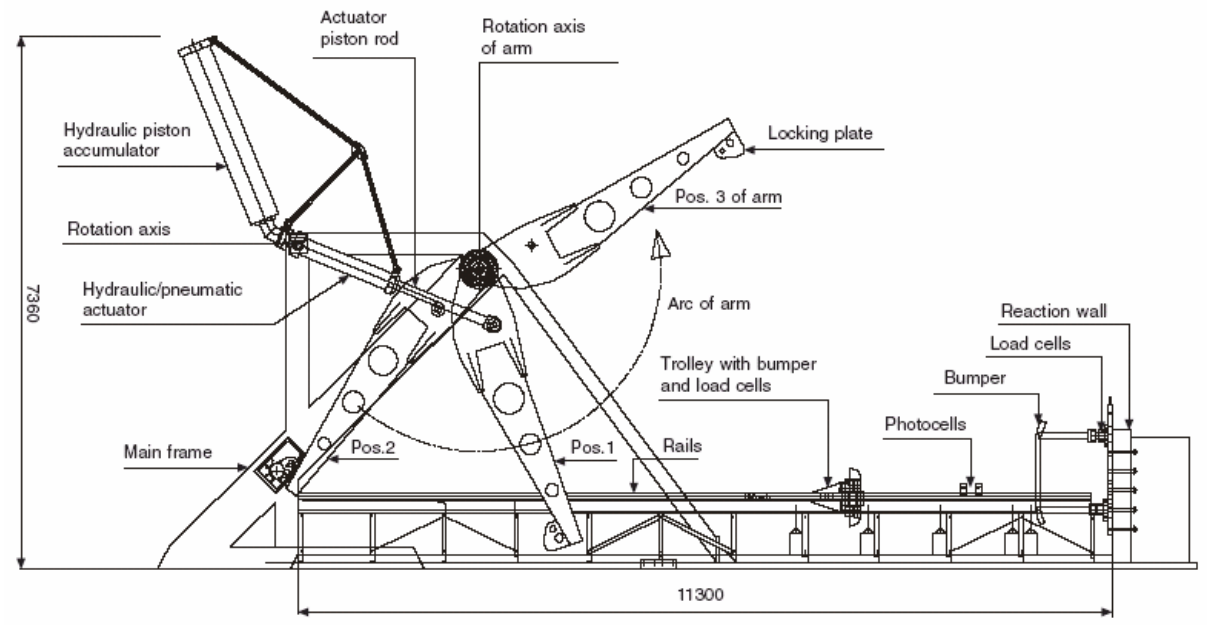

Figure 2: Kicking machine at SIMLab, NTNU.

filtered force-deformation plots for the five parallel tests are shown in Figure 4. Some general observations can be made regarding the deformation pattern of the bumper beam-longitudinal system.

- With high strength longitudinals the impact energy of the trolley is completely absorbed in crushing the bumper beam and the left longitudinal at the impacted end, as well as bending the right longitudinal, without activation of crash boxes on the reaction wall. This system has higher energy absorption capability than the ones with medium and low strength longitudinals.
- A plastic hinge was developed in the mid-section of the bumper beam. At this position, rupture in the folded compression flange and webs of the bumper beam was observed.
- A through-thickness shear failure was observed on the right side cut-out region of the bumper beam.
- All five repetitions showed similar deformation modes as well as force-deformation curves, i.e. a robust performance, see Figure 4.

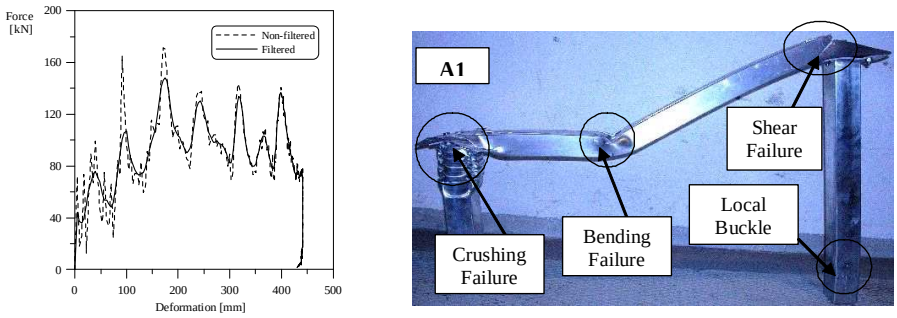

Figure 3: Force-deformation plots and deformed specimen of test **A1** from experiments.

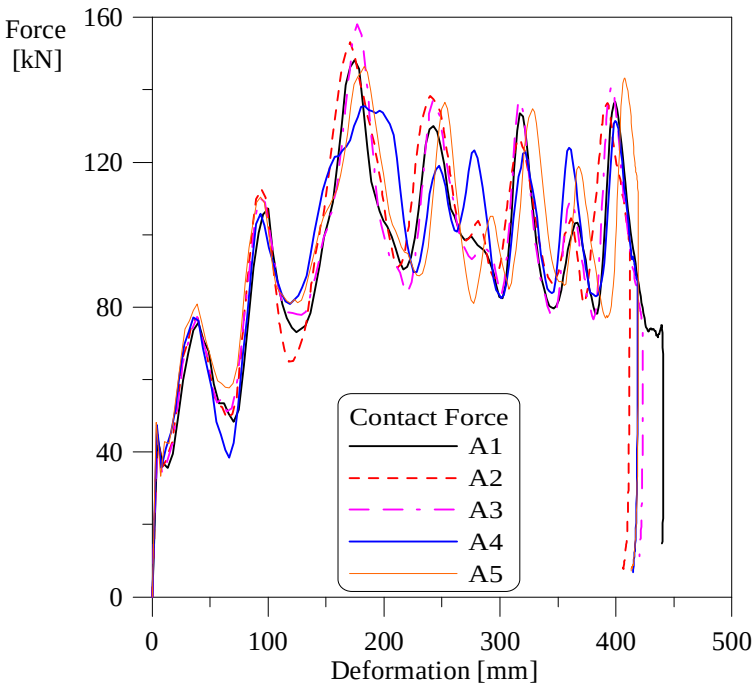

Figure 4: Filtered force-deformation plots for the test series **A**.

4.2 Medium strength longitudinals

The three systems with medium strength longitudinals resulted in significantly different deformation modes i.e. a non-robust performance. The deformed configuration of the bumper beam-longitudinal system for test specimen **B1** along with the non-filtered and filtered force-deformation plots are shown in Figure 5. Filtered force-deformation plots for all the three parallel tests are shown in Figure 6. For this system the following observations are emphasised.

- The deformation mode for the three parallel tests varied significantly and is reflected by the scatter in the force-deformation plots shown in Figure 6. The tendency to unacceptable failure modes in the bumper beam and longitudinal was stronger than for test series **A**.
- The longitudinals in this series had a lower energy absorption compared to test series **A**, due to a different deformation mode and this can be related to the stress-strain behaviour in Figure 9(a). In all the three parallel tests the trolley activated the crash boxes on the reaction wall.
- As with test series **A**, a through-thickness shear failure occurred on the right side cut-out region of the bumper beam.

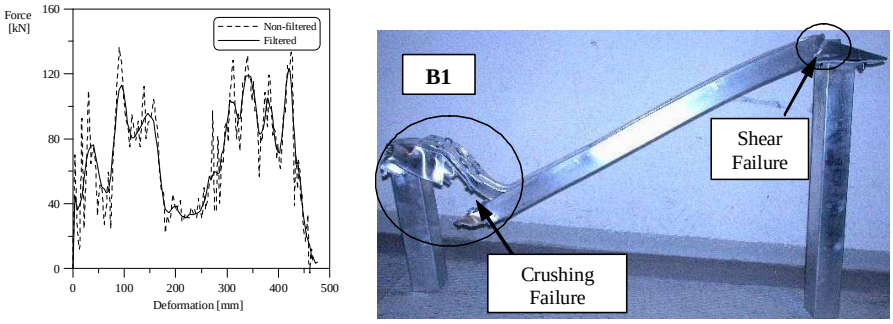

Figure 5: Force-deformation plots and deformed specimen of test **B1** from experiments.

4.3 Low strength longitudinals

The response data obtained from the three parallel test specimens when using low strength longitudinals showed a repeatable deformation mode. The deformed bumper beam-longitudinal system for test specimen **C1** along with the non-filtered and filtered force-deformation plots are shown in Figure 7. All the filtered force-deformation plots for three parallel tests are shown in Figure 8. Some main observations are as follows.

- The longitudinals used here have less strength than the ones used in series **A** and **B**. Consequently, the impact energy absorbed by the bumper beam-longitudinal system is

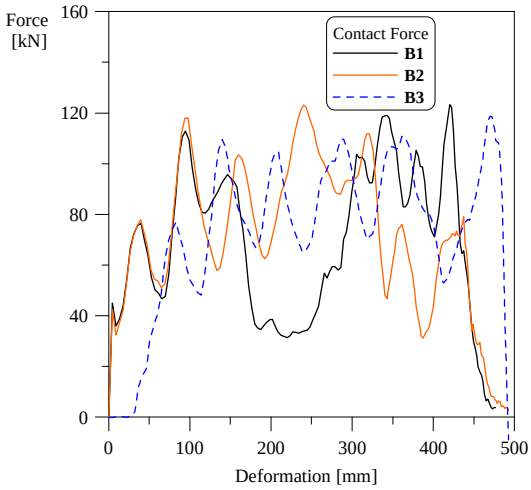

Figure 6: Filtered force-deformation plots for the test series **B**.

much lower. Thus, the crash boxes on the reaction wall were activated in all three tests. The bumper beams are not completely crushed.

- All tests obtained the same deformation mode, namely progressive folding of the longitudinal at the impacted end and with no shear failure on the right side cut-out region of the bumper beam.
- The three tests showed highly repetitive and robust performance.

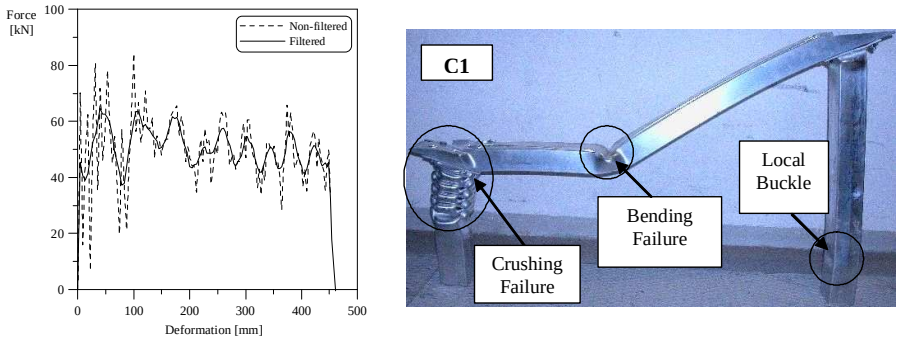

Figure 7: Force-deformation plots and deformed specimen of test **C1** from experiments.

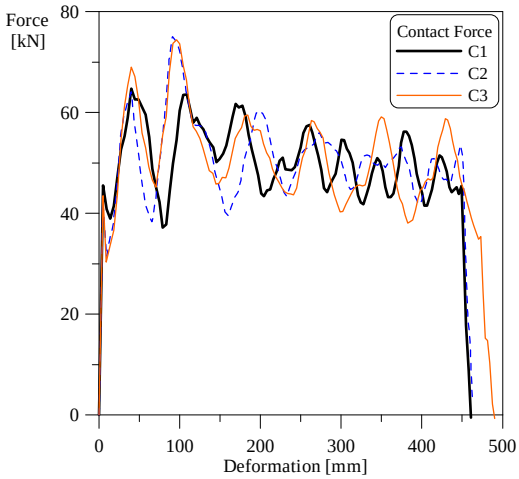

Figure 8: Filtered force-deformation plots for the test series **C**.

5 Material model and parameter identification

The value of numerical analyses is strongly dependent on a validated modelling technology with accurate material models and failure criteria. The traditional way of analysing the bumper beam system is with the assumption of virgin material properties, but this is not true. In practice the bumper beam will undergo a sequence of forming and heat treatment operations before the bumper beam is fitted to the automobile. Due to the forming operations the mechanical and geometrical properties of the cross-section of the bumper beam will change from point to point. Consideration of these process effects in the crash analyses of such systems may play a prominent role.

In the crash analyses of bumper beam-longitudinal systems, shown in Figure 1(a), accuracy, reliability and efficiency are the important criteria for the constitutive models. The above mentioned process effects can be included in the currently adopted user-defined elasto-viscoplastic material model, which incorporates state-of-the-art anisotropic plasticity, associated flow rule, an isotropic strain and strain-rate hardening rule as well as two ductile failure criteria; namely i) Critical Thickness Strain (CTS) [13] and ii) Cockcroft-Latham (CL) [4] criterion. More details about the model can be found in [10] and [3].

The yield function f, which defines the elastic domain in stress space, is expressed in the form

$$f \;=\; \bar{f}(\sigma) - (\sigma_0 + R) \leq 0 \tag{1}$$

where σ_0 is the reference yield stress, R is the strain hardening variable, while the convex function $\bar{f}$ is defined by the chosen yield criterion. In the present work an anisotropic yield criterion (*Yld2003*) that was recently proposed by Aretz [2] has been utilised for accurate and efficient representation of strong anisotropy in the materials [11]. Further, only isotropic hardening has

been considered (i.e. strain-rate-insensitive behaviour), where the strain hardening has been defined by

$$R = \sum_{i=1}^{2} Q_{Ri} \left[1 - \exp(-C_{Ri}\bar{\varepsilon})\right] \tag{2}$$

where $\bar{\varepsilon}$ is the accumulated plastic strain and Q_{Ri} and C_{Ri} are strain hardening constants.

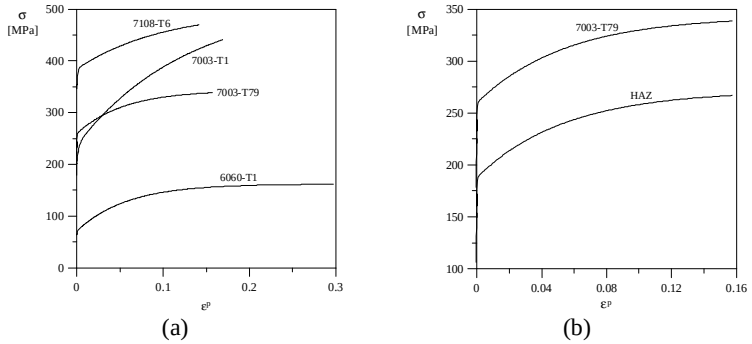

Figure 9: (a) Stress-strain curves identified from uniaxial tensile tests along extrusion direction for relevant alloy and temper conditions, (b) Stress-strain curve used for heat affected zone (HAZ).

Uniaxial tensile tests were performed in three material directions ($\alpha = 0^\circ$, 45° and 90°) with respect to the extrusion direction, measuring force and length strain. For each experiment, true stress and true plastic strain were determined. Figure 9(a) shows the true stress vs. plastic strain curves from uniaxial tensile tests along the extrusion direction, which is chosen as the reference direction. Table 2 summarises the parameters obtained by fitting these result to the generalized Voce strain hardening rule using a weighted least-square approach. In Table 3 the dimensionless anisotropy parameters for the $Yld2003$ criterion have been identified based upon a weighted least-square approach. The critical thickness strain (CTS) [13] determined for the different alloy and temper combinations is also given in Table 2. Further details on the calculation of CTS parameter can be found in Yeh et al. [13].

As mentioned earlier, the interface plate was welded to the longitudinal, thus it was assumed that a softer zone would develop at the welded end in the longitudinal. Hereafter, this softer zone is called a heat-affected zone (HAZ). In the numerical model the HAZ length was modelled with an assumed length of 20 mm based on Eurocode 9 [12]. The stress-strain curve used for the HAZ is shown in Figure 9(b). This is same as that used to represent the base material (longitudinal) but with 30% shift in true stress strain curve according to Eurocode 9 [12]. The failure criterion was not considered for the HAZ in the simulations.

Table 2: Hardening parameters for generalized Voce strain hardening rule and critical thickness strain (CTS) failure criterion [13] values.

Alloy-Temper	α	σ_0 [MPa]	Q_{R1} [MPa]	C_{R1}	Q_{R2} [MPa]	C_{R2}	CTS
AA7108-T6	0 °	347	37.0	1017	113	9.99	0.19
AA7003-T79	0 °	239	20.4	4822	83.7	18.4	0.36
AA7003-T1	0 °	202	35.3	455.9	276	7.89	0.12
AA6060-T1	0 °	63.8	7.13	1403	91.0	17.4	0.63

Table 3: Dimensionless anisotropy parameters in Aretz yield criterion ($Yld2003$) [2].

Alloy-Temper	a_1	a_2	a_3	a_4	a_5	a_6	a_7	a_8
AA7108-T6	0.839	0.979	0.969	1.087	0.855	0.979	1.103	1.161
AA7003-T79	0.980	1.103	1.050	1.154	0.897	1.059	1.116	1.015
AA7003-T1	0.924	1.061	1.001	1.229	0.874	1.035	1.131	1.069
AA6060-T1	0.923	1.029	0.936	1.086	0.932	1.047	0.868	1.062

6 Numerical study

Numerical simulations of the bumper beam-longitudinal systems at 40% offset impact tests were performed using the non-linear FE-code LS-DYNA [1].

6.1 Numerical model

Figure 10 shows the complete FE-model of the test set-up after the assembly of all components. The FE-model was discretized using both shell and solid elements in different parts of the system. The Belytschko-Tsay shell element with one in-plane and five through thickness integration points were used in the bumper beam, longitudinals and interface plates. While in the fixtures and loadcells, the default brick elements were used. The shell element size was approximately 5x5 mm^2, thus, the HAZ in Figure 10, has four elements. The impact velocity was applied through a rigid body modelled with shell elements. The impactor was allowed to move only in the x-direction (see Figure 10) with a given initial velocity of 10 m/s. For the various contact conditions in the bumper beam-longitudinal system, different types of contact algorithms based on penalty method were employed ensuring that no penetrations of the structural parts occurred nor resulting in any numerical robustness problems.

Efforts were taken to model the bumper beam as similar as possible to the reality. Based on the discussion in Section 5, the complete plastic forming operation on the bumper beam (stretch-bending, trimming and hole enlargement) was simulated and the details can be found

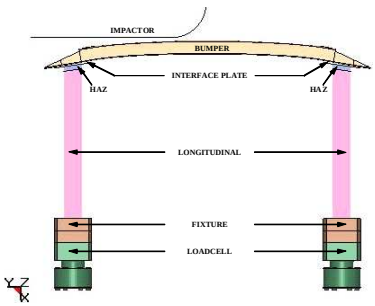

Figure 10: Finite element model of the bumper beam-longitudinal system.

in Kokkula et al. [7]. The obtained bumper beam FE-model only includes the thickness variations resulting from the stretch-bending process. Process effects with respect to material properties are presently not considered. Finally, this stretch-bent bumper beam was studied under 40% offset impact, after assembling all the required components at the respective locations. Furthermore, no strain-rate sensitivity effects were taken into consideration in the present simulations. The simulations were performed on a single Linux processor.

6.2 Numerical results

In the present paper numerical results are summarized only for the bumper beam-longitudinal system with high strength longitudinals, i.e. test series **A**. The simulations are performed using the critical thickness strain failure criterion [4]. In the simulations the kinetic energy of the impactor is converted to plastic work by crushing, bending and stretching of the bumper beam as well as crushing the left longitudinal at the impacted end and also bending the right longitudinal, Figure 12(a). This is similar to that observed in the experiments. In the initial stages of crushing the stretch-bent curved bumper beam starts to flatten, during which the front face and back face of the bumper beam will experience compression and tension stresses respectively. The contact force (at the interface of impactor and the front face of bumper beam) versus time from numerical simulation is plotted against the experimental results in Figure 11(a).

From the force-versus-time curve, Figure 11(a), which is also filtered like the test results with same frequency, several crash events can be identified. The force level in the time from 0 to 10 ms corresponds to the deformation of the bumper beam i.e. collapse of bumper beam cross-section. From 10 to 20 ms the force level is governed by the initiation of the folding mechanism in the left longitudinal at the impacted end. It transpires from Figure 11(a) that the strain localisation during the formation of the first buckle below the HAZ after crushing the bumper beam cross-section was earlier in the simulation compared to the tests. The reason may be the assumed length and mechanical properties of the HAZ. The force level after reaching the maximum peak value, around 20 ms for tests and 15 ms for simulation, drops down significantly, see Figure 11(a). At this time (15 ms) in the simulation the first buckle formation completes in

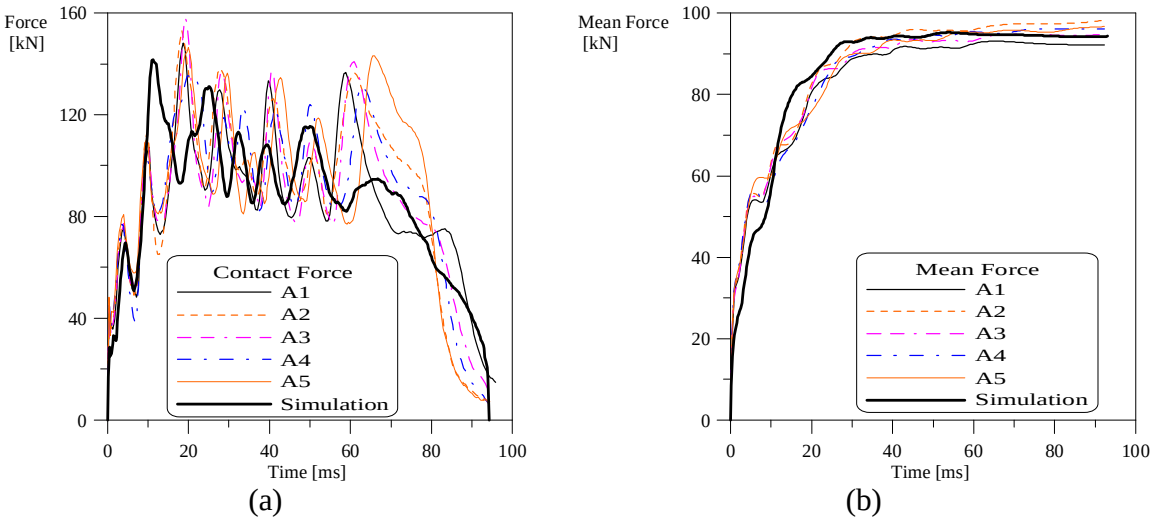

Figure 11: (a) Force-time, (b) Mean force-time curves from tests and numerical simulation.

the longitudinal at the impacted end just below the HAZ, and simultaneously a plastic hinge develops in the mid-section of the bumper beam. The asymmetric loading conditions and also the connection between the bumper beam and longitudinals make the bumper beam to stretch in the axial direction. As the loading at the impacted end continues, the bumper beam curvature will change significantly and strains the right longitudinal considerably. In this position bending of the right longitudinal occurs with the formation of a plastic hinge (local buckle) at the clamped end. As the crash event progresses the left longitudinal folds progressively by absorbing the rest of the kinetic energy of the impactor. The mean force-versus-time plots are shown in Fiugre 11(b). There is excellent agreement between the tests and simulation with respect to the mean force level and thus the energy absorption.

Deformation shapes from the numerical simulation and experimental images are compared in Figure 12. It can be seen from Figure 12(a) that the right longitudinal in the numerical simulation has a more dominant local buckle than in the tests, near by the clamped end of the longitudinal to the fixture. This may be due to the merging of nodes between the longitudinal and the fixture (modelled as a rigid-body). In the tests the longitudinals are fixed inside a rectangular slot in the fixture, using a sliding block mechanism. From Figure 12(b) it is possible to say that the crushing failure mode at the impacted end obtained from simulation is comparable to that in the tests. However, the number of lobes formed in the simulation is one shorter than that in the tests. Bending failure in the middle of the bumper beam is compared in Figure 12(c). In Figure 12(d), it is seen that the shear failure at the right side cut-out region of bumper beam is not predicted in the simulation. The failure which occurred in the tests resembles a through-thickness shear instability mode, but the failure criterion employed in the present simulation is based on a critical thickness strain.

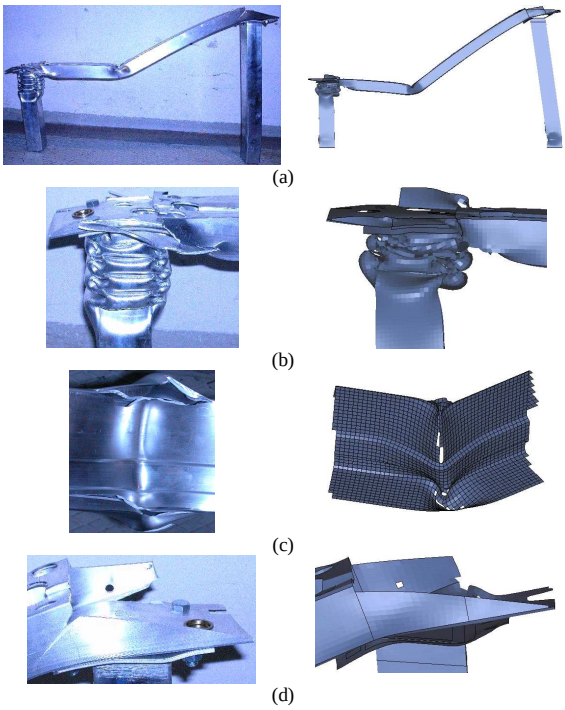

Figure 12: Comparison of deformation shapes for test specimen **A1** and LS-DYNA simulation.

7 Conclusions

The paper presents the crash behaviour of a bumper beam-longitudinal systems at 40% offset impact both experimentally and numerically. A numerical model of the bumper beam was obtained following the industrial process-route, which after assembling with the necessary parts was subjected to impact. Experimental and numerical results were compared for a selected system and the following can be summarized from this study:

- Excellent agreement between the experiments and numerical simulation was found with respect to overall deformation mode and energy absorption. However, in the simulation the maximum peak in the force-versus-time plot occurred earlier compared to tests.
- Overall failure modes in the tests seem to be captured by the simulation with the currently adopted user-defined elasto-viscoplastic material model with critical thickness strain failure criterion.
- Numerical simulation over-predicted the deformations at the right longitudinal in the formation of a local buckle near by the clamped end.

Acknowledgements: This work is financed through the Strategic University Program (SUP), supported by the Research Council of Norway.

References

[1] *LS-DYNA KEYWORD USER'S MANUAL v 970.* Livermore Software Technology Corporation, Livermore; California, April 2003.

[2] H. Aretz. Applications of a new plane stress yield function to orthotropic steel and aluminium sheet metals. *Modelling and simulation in Materials Science and Engineering*, 12:491–509, 2004.

[3] T. Berstad, O. G. Lademo, K. O. Pedersen, and O. S. Hopperstad. Formability modeling with LS-DYNA. In *8th LS-DYNA International Users Conference*, Detroit, 2004.

[4] M. G. Cockcroft and D. J. Latham. Ductility and workability of metals. *Journal of the Institute of Metals*, 96:33–39, 1968.

[5] T. Frank and K. Gruber. Numerical simulation of frontal impact and offset collisions. *CRAY Channels; Cray Research Inc*, pages 2–6, 1992.

[6] A. G. Hanssen, T. Auestad, T. Tryland, and M. Langseth. The kicking machine: A device for impact testing of structural components. *International Journal of Crashworthiness*, 8(4):1–8, 2003.

[7] S. Kokkula. *Bumper beam-longitudinal system subjected to offset impact loading. An experimental and numerical study.* PhD thesis, Department of Structural Engineering, Norwegian University of Science and Technology, Trondheim, 2005.

[8] S. Kokkula, O. S. Hopperstad, O. G. Lademo, T. Berstad, and M. Langseth. Offset impact behaviour of bumper beam-longitudinal system (Part II: Numerical simulations). *Submitted for journal publication*, 2005.

[9] S. Kokkula, M. Langseth, O. S. Hopperstad, and O. G. Lademo. Offset impact behaviour of bumper beam-longitudinal system (Part I: Experimental investigations). *Submitted for journal publication*, 2005.

[10] O. G. Lademo, T. Berstad, O. S. Hopperstad, and K. O. Pedersen. A numerical tool for formability analysis of aluminium alloys. Part I: Theory. *Steel Grips (Suppl Metal Forming 2004)*, 2:427–431, 2004.

[11] O. G. Lademo, K. O. Pedersen, T. Berstad, and O. S. Hopperstad. A numerical tool for formability analysis of aluminium alloys. Part II: Experimental validation. *Steel Grips (Suppl Metal Forming 2004)*, 2:433–437, 2004.

[12] prEN 1999-1-1. Eurocode 9: Design of aluminium structures. Part 1.1: General structural rules. *CEN, rue de Stassart 36; B-1050 Brussels; (Stage 34)*, May 2004.

[13] J. R. Yeh, T. L. Summe, and D. C. Seksaria. The development of an aluminium failure model for crashworthiness deign. In Barbat Mahmood and Baccouche, editors, *Crashworthiness, Occupant protection and Biomechanics in Transportation systems*, New York, 1999. ASME.